Available online at www.sciencedirect.com
SCIENCE DIRECT®
Acta Materialia 52 (2004) 3483–3492
Acta MATERIALIA
www.actamat-journals.com

Competition between grain boundary segregation and Cottrell atmosphere formation during static strain aging in ultra low carbon bake hardening steels

B. Soenen [a,*], A.K. De [b], S. Vandeputte [a], B.C. De Cooman [c]

[a] *OCAS N.V., Steel Research Centre, Substrate Development, ARCELOR Group, J. Kennedylaan 3, B-9060 Zelzate, Ghent, Belgium*
[b] *ASPPRC, Department of Metallurgy and Materials Engineering, Colorado School of Mines, 1500 Illinois Street, Golden, CO 80401, USA*
[c] *Laboratory for Iron and Steelmaking, University of Ghent, Technologiepark 9, Ghent 9052, Belgium*

Received 11 September 2003; received in revised form 29 March 2004; accepted 30 March 2004
Available online 6 May 2004

Abstract

A finite differences model has been developed for simulation of carbon segregation to grain boundaries during continuous annealing (CA) of ultra low carbon bake hardening steels. Continuous cooling experiments with variation of soaking times and cooling rates were performed. The solute carbon content was measured by internal friction. The simulation results are in good agreement with the experimental results, using a maximum grain boundary carbon site density of $4/a^2$, with a the unit cell length of bcc-Fe. This value is about four times higher than the literature value reported by McLean and implies that far more carbon can be stored in grain boundaries than formerly expected. Competition between carbon diffusion to grain boundaries and to dislocations during subsequent strain aging of the material was modelled with Monte-Carlo simulations. Using the same parameter values for the grain boundary site density as during CA, the simulations were also in good agreement with strain aging experiments.

Keywords: Aging; Diffusion; Dislocations; Grain boundaries; Segregation; Kinetics

1. Introduction

Static strain aging in ultra low carbon (ULC) steels is an interaction process of the dislocations and carbon atoms due to the elastic strain field associated with both of them. When prestrained specimens of ultra low carbon steels are aged at low temperatures, the kinetic energy kT gained by the solute carbon atoms causes them to diffuse to the dislocations and thereby relieve the stress field around the dislocations through formation of an atomic atmosphere called the ''Cottrell atmosphere'' [1]. The segregation of carbon atoms to the dislocations immobilises the dislocations to take further part in the subsequent yielding process. The most immediate manifestation of the pinning of the dislocations is the increase in the upper yield stress of the aged specimens and the appearance of a yield point elongation, visible as Lüders bands, in a classical tensile test [2,3]. The use of controlled aging during paint baking in deformed material is known as ''bake hardening'', and has led to the development of a number of commercial steel grades.

Cottrell has shown that the kinetics of strain aging is dependent on the amount of solute carbon and the number of free dislocations. In addition to this, it can be assumed that this process is in competition with the segregation of carbon to the grain boundaries, a process that lowers the solute carbon. Furthermore the amount of solute carbon at the start of strain aging in ULC steels can already differ from the overall carbon content, depending on carbon segregation to the grain boundaries during preceding thermal cycles such as continuous annealing (CA).

To study the influence of segregation processes during CA and subsequent strain aging, extensive experi-

* Corresponding author. Tel.: +32-9-345-13-34; fax: +32-9-345-12-04.
E-mail address: bart.soenen@arcelor.com (B. Soenen).

1359-6454/$30.00 © 2004 Acta Materialia Inc. Published by Elsevier Ltd. All rights reserved.
doi:10.1016/j.actamat.2004.03.046

mental research was done [4], and this work was compared with computer simulation results to determine the influence of several parameters, including the grain size and the carbon site density in the grain boundary.

The latter parameter is particularly not well quantified. Most literature data about grain boundary occupation of carbon is obtained with Auger electron spectroscopy, where the Auger electrons of the outer layers of the grain surface are measured [5–7]. The material is fractured, but because carbon in the grain boundaries increases the cohesive strength, phosphorous or sulphur are added to promote intergranular fracture. To know the number of carbon atoms which is at the grain boundary, the C Auger signal is then compared with the Fe Auger signal. To do this comparison properly, several factors have to be taken into account:

- The sensitivity of the detector for both elements.
- The escape depth of Auger electrons for both elements, assuming that the escape depth is much smaller than the penetration depth of the primary electrons.
- A model for the thickness distribution of the carbon atoms in the upper layers.

Most authors do not take into account the two last factors and don't arrive at a determination of the amount of carbon at the grain boundary. Suzuki et al. [5] however takes into account the escape depths, and assumes that the carbon atoms are located in a 2.5-Å thick boundary volume. He obtains concentrations of 20 at.% carbon in this volume, which corresponds to a surface site density of $0.5/a^2$, with a is the lattice unit cell length (2.87 Å) of bcc-Fe. This number depends on the assumed thickness of the boundary volume. In a review study, McLean [8] discusses the phenomenon of grain boundary segregation of substitutional and interstitial atoms. He estimates the grain boundary as 3 atoms thick. At saturation, one-third of the sites contain solute atoms, which corresponds to a grain boundary site density of $1/a^2$, or monolayer coverage. A major goal of this study is to asses the maximum amount of carbon that can be stored in the ferrite grain boundaries, for a given composition. The general approach to asses the carbon grain boundary density will be fitting of simulations to different experimental results, i.e. internal friction measurements and strain aging data.

From the preceding literature overview, it is clear that phosphorous and sulphur can influence the maximum amount of carbon that can be stored in the grain boundary. Indeed, it has be shown that phosphorous and sulphur compete with carbon for the same grain boundary sites [9]. In our material, the solute sulphur content is extremely low, due to the presence of Mn, which forms MnS. In [9], a study of the grain boundary segregation competition between carbon and phosphorous revealed that carbon has a higher segregation energy, and tends to replace phosphorous at the grain boundaries, certainly for the moderate phosphorous levels present in the steel studied here. For higher phosphorous levels, this is not longer true, so the presented results are only valid for this P content.

2. Modelling

In a first step, the carbon segregation to the grain boundaries during CA was studied. A computer simulation model was developed to solve the diffusion equation with the appropriate boundary conditions. Assuming the grains to be spherical in shape, the diffusion equation is given as

$$\frac{\partial c}{\partial t} = D\left(\frac{2}{r}\frac{\partial c}{\partial r} + \frac{\partial^2 c}{\partial r^2}\right), \tag{1}$$

where $D = D_0 \exp(-U_d/RT)$ is the diffusion coefficient (m^2/s), r is the radial distance (m), and c is the carbon atom-fraction. The following boundary conditions are set for a mirror condition for the flux in the grain centre and the McLean equation for the concentration at the grain boundary considering local equilibrium [10]:

$$J_r(0) = 0, \tag{2}$$

$$c(r_g) = \left(\frac{\theta}{1-\theta}\right)\frac{1}{\exp(-U_s/RT)}, \tag{3}$$

where r_g is the grain radius, θ the coverage and U_s the segregation energy. In the model, the grain boundary is represented by an infinitesimally thin layer which consists of sites where carbon atoms can be stored. The coverage is the number of segregated atoms in the grain boundary divided by the total number of grain boundary atom sites where carbon can be located. The latter number has a maximum of M/a^2 per unit grain boundary area. M is a parameter that can be adjusted in the model. It should be noted that a one-grain model was developed, so every value obtained for M should be multiplied by two to obtain the grain boundary site density, to take into account the fact that a grain boundary as commonly defined in the literature is shared by two grains. The diffusion equation is numerically solved with finite differences. An explicit method is used for calculating the time derivative. For the simulations, the following reference values for carbon in bcc-Fe were used: diffusion coefficient $D = 2 \times 10^{-6} \exp(-84\,140/RT)$ m^2/s [11] and the segregation energy $U_s = -57\,000 - 21.5T$(K) J/mol [10]. Alternatively, since the parameter M is a fitting parameter in the present model, it can be adjusted to match with the actual carbon concentration in the specimens from experimental results. The model does not consider the precipitation reactions that might take place during the cooling process. However, since the total amount of carbon is very low in the present case and a fast cooling rate is

applied, it is assumed that no precipitation involving carbon takes place. As will be seen later, low temperature carbides can precipitate during the baking stage which can transform into cementite after prolonged aging times [12].

In a second step, the dynamics of Cottrell atmosphere formation was calculated with Monte-Carlo simulations that occurs after straining, when new free dislocations are created. The advantage of the Monte-Carlo method is that (i) it allows the system to evolve to thermal equilibrium by successive arbitrary steps with transition probability P [13] and (ii) it allows one to use a poorer symmetry (e.g. random distribution of dislocations inside the grain). The probability P satisfies the following condition to ensure approach to thermal equilibrium,

$$P(\mathrm{A} \rightarrow \mathrm{B}) = P(\mathrm{B} \rightarrow \mathrm{A}) \exp\left(\frac{U_\mathrm{A} - U_\mathrm{B}}{RT}\right), \tag{4}$$

where U_A and U_B are the internal energies of the system in states A and B, respectively. The simulations were two-dimensional and performed in a rectangle containing an orthogonal grid. The grid cell edge was taken as a. At the boundaries of the rectangle, mirror conditions are applied. One side of the rectangle was chosen as the grain boundary and every carbon atom positioned there has an energy U_s compared to the bulk. The other edge of the rectangle was taken as the radius of the grain. In the bulk, edge dislocations were randomly placed at the edges of the cells. The average spacing between the dislocations was taken as $\rho^{-1/2}$ [14]. Carbon atoms were positioned in the middle of the unit cells. A carbon jump in the bulk or to a grain boundary site is one Monte-Carlo step, and in the following the expressions for each kind of jump will be constructed.

In the bulk, far from dislocations, carbon atoms can jump from cell i to one of the four neighbouring cells j with a jump frequency $f(i \rightarrow j)$. If there is no energy difference between two adjacent positions i and j, then the jump frequency can be derived from the diffusion coefficient $D = D_0 \exp(-U_\mathrm{d}/RT)$ [15,16]:

$$f = f_\mathrm{d} = v \exp\left(-\frac{U_\mathrm{d}}{RT}\right), \quad v = \frac{D_0}{a^2} \tag{5}$$

with f_d consisting of an attempt frequency v (s^{-1}) to move to an adjacent site and a probability to surmount the energy barrier U_d (J/mol).

Besides ("normal") carbon diffusion between positions with equal internal energy, carbon diffusion to dislocations has been considered. The interaction energy, U_c between a solute atom and the hydrostatic component of the stress field of an edge dislocation is given by Cottrell [17]:

$$U_\mathrm{c}(r,\theta) = \frac{A \sin\theta}{r}, \tag{6}$$

where (r,θ) is the polar co-ordinate of the solute atom with respect to the dislocation line and A is the solute-dislocation interaction parameter. Based on Eq. (6), the interaction energy at different atomic positions around the edge dislocation (Fig. 1) can be calculated as shown in Table 1. For the case of carbon in bcc-iron, Cottrell and Bilby [1] estimated A to be 1.8×10^{-5} J m/mol. However, a value of 7.5×10^{-6} J m/mol for A was used in the present model because in the geometry around the edge dislocation the atom in the most stable position then has a binding energy of −52 kJ/mol which is close to the experimentally reported value for A [18,19]. A dislocation introduces an extra energy $A\sin\theta/r$ at every position in the infinite lattice. So, inside the stress field of the dislocation, the jump frequency of carbon atoms varies with the jump direction. Jumps to a position of higher energy or to a position of lower energy are governed by the following respective equations:

$$f(i \rightarrow j) = f_\mathrm{d} \exp\left(\frac{U_i - U_i}{RT}\right), \quad U_i < U_j, \tag{7}$$

$$f(i \rightarrow j) = f_\mathrm{d}, \quad U_i > U_j. \tag{8}$$

It is important to note from the above deliberations that the jump frequency will show a strong anisotropy in the neighbourhood of a dislocation. The energy difference between adjacent positions varies as r^{-2} and becomes much smaller than the diffusion barrier at large distance

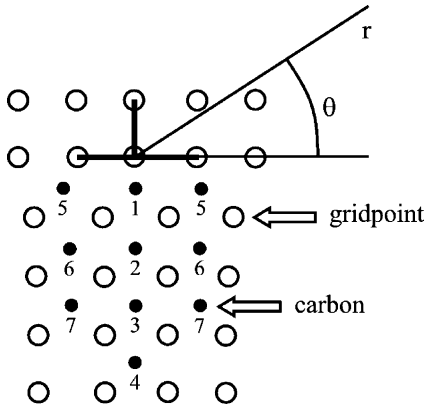

Fig. 1. Atomic positions of interstitial carbon around a positive edge dislocation.

Table 1
Interaction energies at different sites in the neighbourhood of an edge dislocation

Site	U_c	Energy (kJ/mol)
1	$-2A/a$	−52
2	$-2A/3a$	−17
3	$-2A/5a$	−10
4	$-2A/7a$	−7
5	$-2A/13a$	−10
6	$-6A/13a$	−12
7	$-10A/29a$	−9

from the dislocations. Hence, a critical radius r_c of the circle allowing for a maximum jump frequency variation of 10% has been taken into account in the model. Inside of this area Eqs. (7) and (8) are valid. The critical radius is given by

$$r_c \geqslant \sqrt{\frac{2Aa}{RT\ln(1.1)}}. \tag{9}$$

Outside this circle, the jump frequency is governed by "normal" diffusion.

Finally, the jump frequency for jumping from the bulk to the grain boundary and from the grain boundary to the bulk was modelled as follows:

$$f(\mathrm{GB} \rightarrow \mathrm{bulk}) = f_d \exp\left(\frac{U_s}{RT}\right), \tag{10}$$

$$f(\mathrm{bulk} \rightarrow \mathrm{GB}) = f_d. \tag{11}$$

The dynamics of the system of atoms is calculated by repeating the following algorithm:

1. From the list of atoms, one particular atom will jump first. Suppose this is atom p.
2. The simulation time is put equal to the cumulative jump time t_p.
3. A random number q between 0 and $g(p,4)$ is generated, with $g(p,k) = \sum_{l=1}^{k\leqslant 4} f(p,l)$. Based on this number, the direction k of the jump is determined: $g(p,k-1) \leqslant q \leqslant g(p,k)$. The atom is moved in this direction to the adjacent cell. If the cell is already occupied, the atom is not moved. Thus the model exclusively takes into account the saturation effects i.e., a change of the interaction energy throughout the aging process is not allowed. The atmosphere density at saturation was assumed as consisting of one carbon atom per lattice plane threaded by the dislocations [1].
4. The jump frequencies $f(p,k)$, $k = 1 \rightarrow 4$ in the new position are calculated.
5. The cumulative jump frequencies $g(p,k)$ in the new position are calculated.
6. The atom jump time $\tau_p = 1/g(p,4)$ is calculated. The cumulative atom jump time is updated with $t_p = t_p + \tau_p$, and the atoms are sorted to their cumulative jump time.

This cycle is repeated for a certain period and the value of the degree of saturation of the dislocations is evolved during the simulations. The degree of saturation at any time t is defined as the number of carbon atoms arriving at the dislocation sites 1 (position 1, see Fig. 1) to the total number of dislocation sites 1 assumed at $t = 0$.

In order to validate the model, the increase in yield stress was measured, and it can be shown that it varies exponentially with the saturation of the dislocations. Following Hartley [20], if a single deformation mechanism is operating during prestraining and retesting after aging, for a constant strain rate it can be written

$$\dot{\epsilon}_p = b\rho s v^* \exp\left(-\frac{H_0 - v_0(\sigma - \sigma_\mu)}{kT}\right), \tag{12}$$

where v^* is the frequency of vibration of the dislocation involved in the yielding process, s is the average distance a dislocation moves after every thermal activation, H_0 is the activation barrier, v_0 is the activation volume of the dislocation structure associated with the deformation process, σ_μ is the internal stress of the material. Hence, if ρ_x and σ_x are the mobile dislocation density and the flow stress at the end of x% prestraining and ρ_a and σ_a are the dislocation density and the yield stress after aging for time t then from Eq. (12)

$$\frac{\rho_a}{\rho_x} = \exp\left(\frac{v_0(\sigma_x - \sigma_a)}{kT}\right) = \exp\left(-\frac{v_0\Delta\sigma}{kT}\right) \tag{13}$$

or

$$\frac{\rho_x - \Delta\rho(t)}{\rho_x} = \exp\left(-\frac{v_0\Delta\sigma}{kT}\right) \tag{14}$$

or

$$\frac{\Delta\rho(t)}{\rho_x} = 1 - \exp\left(-\frac{v_0\Delta\sigma}{kT}\right). \tag{15}$$

Here $\Delta\rho(t)$ is the length per unit volume of the dislocations pinned by the carbon atoms in time t, hence $\Delta\rho(t)/\rho_x$ is the degree of formation of the atmosphere at time t. Eq. (15) gives a functional relationship between the degree of formation of the atmosphere with time t and the corresponding increase in the yield stress. To calculate the time dependence of $\Delta\rho(t)$, the number of carbon atoms arriving at the dislocation centre at time t has to be derived.

3. Experimental

The compositions of the two steels are listed in Table 2. Steel A is used for studying the influence of the CA cycle on the bake hardening kinetics. Due to lack of material A, a second heat B had to be cast with the same aimed composition. Steel B is used for looking at the influence of the prestrain and the aging temperature on the hardening.

Samples were annealed, prestrained and aged at various temperatures specified hereunder. To determine the bake hardening value, specimens were measured before and after aging. The increase in the yield stress,

Table 2
Chemical composition of the steel (wt. ppm)

	C	Mn	P	S	Al	Ti	N
Steel A	24	900	450	30	490	70	16
Steel B	20	900	450	30	490	70	16

$\Delta\sigma$, due to the aging was measured as the difference between the flow stress at the end of prestraining and the upper yield stress after aging for time t. The original specimen dimensions were used in measuring the stresses to ensure that the increase in the yield stress is due solely to the carbon segregation to the dislocations.

The solute carbon content in the specimens was measured by internal friction using a variable frequency and a variable temperature method. In this study the solute carbon content is defined as the carbon in the ferrite matrix but does not include the carbon in the grain boundary. Frequency variation was obtained with a torsion pendulum (TP) operated at 2 kHz. Temperature variation was obtained with a piezoelectric ultrasonic composite oscillator (APUCOT) [21] operating at 40 kHz. The internal friction due to the stress induced ordering of interstitials is determined at a stress amplitude of 10^{-7} during the fast heating (100 °C/min) of the specimen in the range of 20–300 °C. The advantage of this technique is that it can measure the Snoek peak for ultra low levels of carbon in specimens due to a high signal to noise ratio. However, if the dislocation density is high in the specimens then there is a possibility of carbon atoms segregating to the dislocations during the measurement. Therefore for quantitative use, torsion pendulum results will be considered in the present work, whereas APUCOT is more used for qualitative interpretations, e.g. indicating trends.

3.1. Variation of the soaking time during CA

Different CA cycles were applied for the cold rolled sheets of steel A to vary the solute carbon content by variation of the grain size. The annealing cycle was carried out in a salt bath furnace with inhibitor addition to prevent decarburization. The hot rolled sheets were given 70–80% cold reduction, annealed at 850 °C for 2–20 min and then water quenched to room temperature. Four different grain sizes were produced. A linear intercept method was used to measure the grain sizes. The intercepts were multiplied with a correction factor 1.5 to obtain the physical 3-D grain size [25]. For this correction a spherical grain was assumed, but optical microscopy confirmed that indeed a spherical grain was present after annealing. The grains were reasonably uniform in all the specimens and the average grain diameters measured were 21, 26, 44 and 66 μm. Tensile specimens prepared out of these sheets were prestrained 5% and then aged at 50 °C for different times.

3.2. Variation of the cooling rate after CA

A second method to vary the solute carbon content in the steel was obtained by varying the cooling speed after soaking. This annealing cycle was done in a Gleeble 1500/20 continuous annealing simulator. The soaking was 60 s at 850 °C and a grain size of 26 μm was obtained. Beside a water quenching (WQ), fast cooling (50 °C/s) and slow cooling (11 °C/s), including an overaging cycle at 400 °C for 180 s, were applied. Tensile specimens prepared out of these sheets were prestrained 5% and then aged at 50 °C for different times.

3.3. Variation of the temperature during strain aging

Hot rolled sheets of steel B were given 75% cold reduction and then annealed at 850 °C for 60 s followed by an overaging cycle at 400 °C for 180 s. A cooling rate of 11 °C/s was used during the annealing. The annealed sheets were further subjected to a skin pass reduction of 1.3%. The skin pass is the final small rolling pass after annealing to eliminate a remaining yield point elongation and to provide the final roughness in industrial practise. The average grain size of the annealed sheet was 26 μm. The solute carbon content was about 6 ppm as measured by internal friction method (TP). Tensile specimens made out of these sheets were prestrained 5% and then aged at temperatures between 50 and 170 °C for different times in a silicone oil bath.

3.4. Variation of the prestrain

Tensile specimens prepared from the above sheets were given a tensile prestraining of 1–10% to vary the dislocation density in the specimens, and then aged at 50 °C for varied times to study the effect of prestrain on the atmosphere formation.

4. Results and discussions

4.1. Variation of the soaking time during CA

Fig. 2 shows the internal friction spectra obtained in the specimens with different grain sizes, after water quenching. The peak height decreases with decreasing grain size, implying a decrease in the solute carbon content. The actual matrix carbon contents measured by APUCOT are lower than the amount measured with torsion pendulum, which is due to the fact that the internal friction peak is obtained at temperatures around 190 °C. During the heating period (about 100 s) to the peak temperature, solute carbon diffuses to the dislocations generated during quenching from the annealing temperature. The presence of mobile dislocations in the water-quenched specimens was evident from the absence of any yield point elongation during the tensile prestraining of these specimens.

Figs. 3 and 4 show the numerical simulation of carbon concentration profiles from the grain centre to the grain boundary and the coverage of the grain boundary as a function of the grain size variation in the specimens.

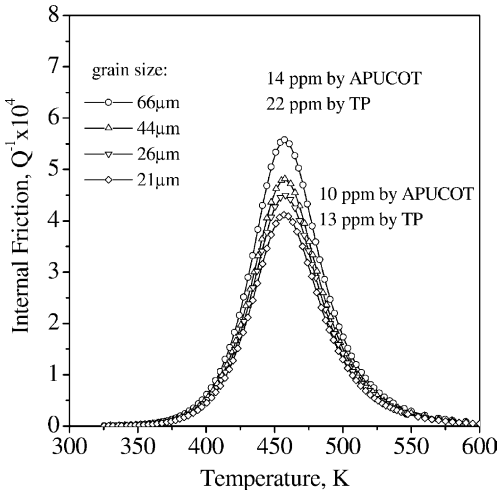

Fig. 2. APUCOT internal friction spectra and torsion pendulum data as a function of grain size (Steel A, water quench cycle).

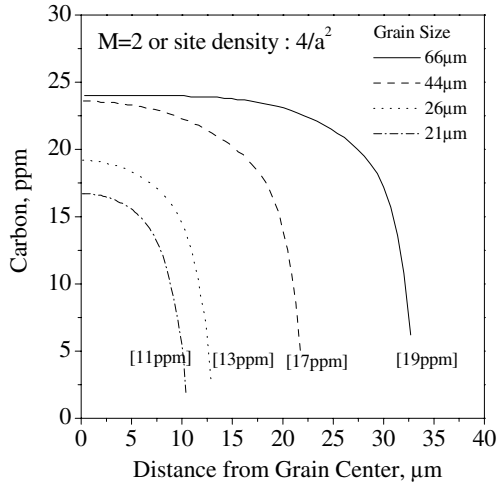

Fig. 3. Numerical simulation of carbon concentration profiles for different grain sizes as a function of the radial distance after the CA cycle (Steel A, water quench cycle). Figures in brackets indicate the mean carbon concentration in the grain.

Fitting of the calculated mean carbon concentrations over the grain interior with the TP internal friction experiments (which do not measure the grain boundary carbon, only the solute matrix carbon) led to the use of $M = 2$ for the simulations, corresponding to a maximum grain boundary carbon site density of $4/a^2$. This high value suggests that the grain boundary consist of more than one atomic layer. However, this was considered to be physically realistic. This value is considerably higher than the value found by Suzuki [7]. It is seen that for a grain size of 66 μm (or higher) almost all the carbon atoms are retained in solid solution. The concentration profile is quite uniform from the grain centre to the grain boundary compared to those in the finer grains. The solute carbon in the matrix decreases with a decrease in grain size, because of the higher total amount

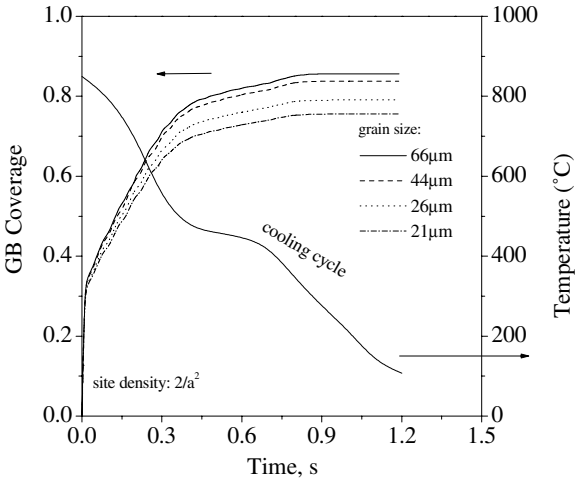

Fig. 4. Numerical simulation of the grain boundary coverage of carbon during the cooling cycle from the annealing temperature (Steel A, water quench cycle). The temperature profile is experimentally recorded during the water quenching, and includes a plateau due to the instability of the vapor film.

of carbon segregated to the larger grain boundary area. Even after the water quenched cooling cycle, the grain boundary coverage is high for all the grains (Fig. 4), which means that the majority of the grain boundary sites is occupied by the carbon atoms. There is a maximum difference in coverage of about 10% between the investigated grain sizes, so the difference in carbon content in the matrix can be accounted for mainly due to the direct effect of change in grain boundary area. It is concluded that for typical industrial grain sizes of 20–30 μm, the amount of segregated carbon can be more than 10 ppm, which is far from negligible in relation to the 20 ppm of carbon present in ultra low carbon steels.

The strain aging behaviour of these specimens are summarized in Fig. 5. From this figure, we can observe that the increase in yield strength consist in two stages. In the first stage the yield strength increases up to 30 MPa and the yield point elongation returns. This first stage is assumed to be the Cottrell atmosphere stage. In the second stage only the yield point increases. As shown in [12], this second stage is probably related with the nucleation and growth of low temperature carbides (<75 °C) or ϵ-carbides (>75 °C), and will be denoted in the following text as the precipitation stage. It will be shown that the maximum increase in the yield stress due to the Cottrell locking is ≈30 MPa in this steel at all the aging temperatures and this is also not influenced by the amount of prestrain (1–10%) or the solute content [3]. Hence to interprete the experimental results expressed as strength values in terms of degree of atmosphere formation, the degree of atmosphere formation at any aging time and temperature has been considered as the fractional increase in the yield stress $\Delta\sigma/\Delta\sigma_{atm}$ with $\Delta\sigma_{atm}$ as 30 MPa. The variation of the solute carbon

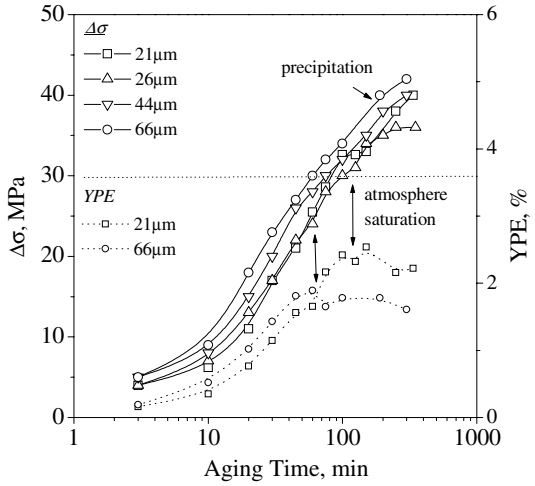

Fig. 5. Increase in yield stress and yield point elongation due to aging at 50 °C in specimens with different grain sizes (Steel A, water quench cycle). The line at 30 MPa indicates the maximum strength increase after the Cottrell atmosphere formation stage.

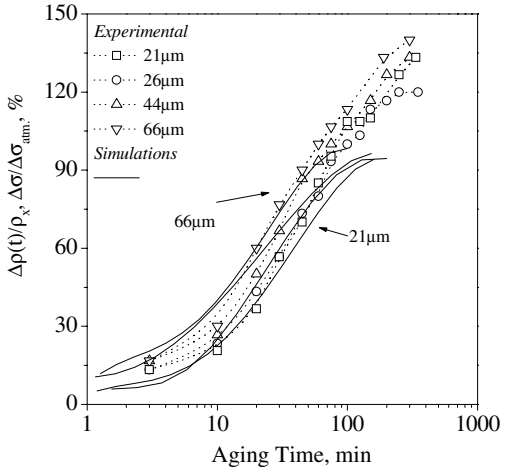

Fig. 6. Comparison of calculated and experimental dislocation saturation evolutions with aging time (Steel A, water quench cycle, 50 °C, prestrain of 5%) as a function of grain size.

content due to the difference in grain size clearly influences the strengthening behaviour during strain aging. The results reveal the following:

1. the yield stress increase due to aging at any stage of the aging period is higher in the coarse-grained specimens,
2. the completion of the first stage of aging (which is marked by the yield point elongation behaviour) is faster with increase in grain size.

The amount of carbon per unit volume of the dislocation stress fields is higher in coarse-grained specimens compared to that in the fine-grained specimens and hence at any specific time of aging the dislocations in the coarse-grained specimens are saturated faster. More details about the Cottrell atmosphere formation stage as well as the precipitation stage can be found in [12] or [22].

Finally, the simulated carbon concentration profiles after the processing were used as input data for the strain aging modelling and fitting. The precipitation stage is not taken into account because there is no accurate nucleation model available yet. Thus, comparing the strain aging results with the calculations, only the first atmosphere formation stage has to be considered (The precipitation of low-temperature carbides or ϵ-carbides on the dislocations can in principle start if this saturation is higher than one.). In agreement with [1], it is also assumed here that there is a linear relationship between the dimensionless strength increase and the dislocation saturation during the Cottrell atmosphere formation stage. For the calculations, a dislocation density of 5×10^{-13} m^{-2} was used for the prestrain of 5% [23].

The results are shown in Fig. 6. The best fitting results were obtained with an activation energy for the carbon diffusion of 82000 J/mol which is in very good agreement with the value of 84 140 J/mol mentioned by Wert and Zener [24]. The CA simulations were redone with this slightly adapted value but it had almost no impact on the initially used grain boundary segregation results. It is noticed that for the atmosphere formation stage an overall good matching is obtained between the simulations and the experiments.

4.2. Variation of the cooling rate after CA

Fig. 7 shows the simulated carbon concentration profiles in specimens with different cooling rates from the annealing temperature. The grain size was about 26 μm for all the specimens. An increase of the cooling

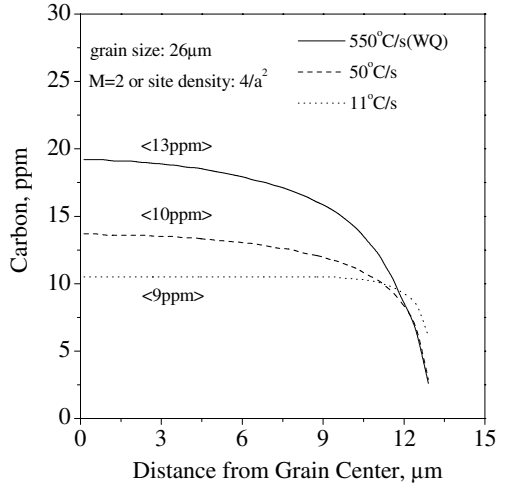

Fig. 7. Simulation of carbon concentration profiles as a function of the radial distance after the CA cycle for different cooling rates (Steel A, grain size 26 μm). Figures in brackets indicate the mean carbon concentration in the grain.

rate leads to a higher solute carbon content in the bulk of the grain. The same maximum grain boundary carbon site density of $4/a^2$ as used for the calculations of Fig. 3 again leads to a good agreement with the torsion pendulum results from Fig. 8. Only for the slow cooling cycle, a larger deviation occurs. Moreover, in the APUCOT result for this cycle, a dramatic decrease in the matrix carbon content is observed after heating up the sample to the Snoek peak temperature. It is thought that the slow cooling rate, resulting in the maximum grain boundary coverage (Fig. 9), allows the start of grain boundary carbon precipitation, not taken into account in the present model. Experimental TEM work on thin foils was not successful in proving this hypothesis, which does not mean that it can be excluded, in view of the expected very small size of these precipitates. Homogeneous precipitation in the matrix (without prestraining) is unlikely in the ULC steels due to the ultra low level of carbon [26,27]. In Fig. 9, the simulations of the grain boundary coverage evolution during the thermal cycle show that the final coverage is higher if the specimen is cooled slower, as can be expected. The final grain boundary coverage with slow cooling remains the same with or without the presence of the overaging step in the annealing cycle.

Fig. 10 gives an illustrative summary of the influence of the cooling rate on the strain aging behaviour of the ULC bake hardening steel. It is seen that the solute carbon in the specimens cooled slowly (11 °C/s) is just sufficient to complete the atmosphere formation. The atmosphere saturation was marked distinctly by the yield point elongation behaviour. The precipitation stage or the second stage of hardening is virtually absent. An increase of the cooling rate increases the solute carbon content in the matrix of the specimens and results in (i) a faster completion of the first stage or the atmosphere saturation stage and (ii) the appearance of a precipitation stage with a significant increase of the yield stress. The maximum bake hardening is obtained in the water quenched specimens because of the highest retention of carbon in the matrix. Fitting of the dislocation saturation calculations with the strain aging experiments as a function of cooling rate led again to an overall good agreement. It is evident from the results that the variation in cooling rate after CA has a pronounced effect on the diffusion of carbon to the grain boundary, explaining bake hardening differences of the same material processed on different industrial lines. Thus, a significant increase of the bake hardenability of the ULC bake hardening steels can be achieved through both a coarse grain size and a faster cooling rate after soaking.

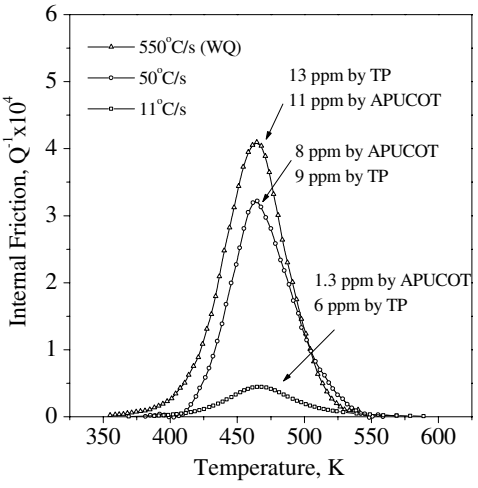

Fig. 8. APUCOT internal friction spectra and torsion pendulum data as a function of cooling cycle (Steel A, grain size 26 μm).

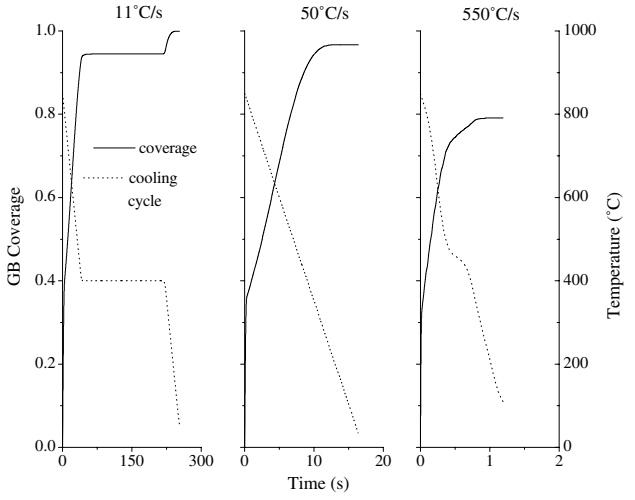

Fig. 9. The grain boundary coverage of carbon during the cooling cycle from the annealing temperature (Steel A, grain size 26 μm).

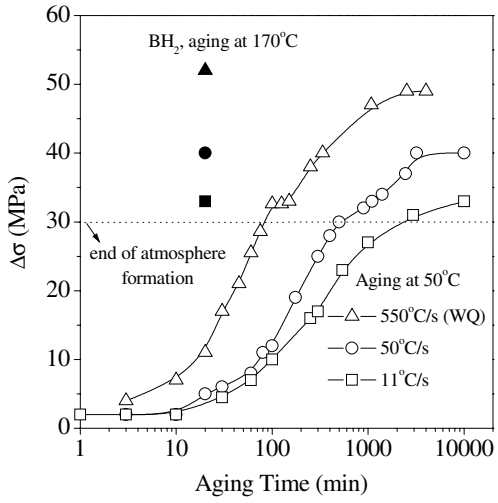

Fig. 10. Comparison of calculated and experimental dislocation saturation evolutions with aging time (Steel A, grain size 26 μm, 50 °C, prestrain of 5%) as a function of cooling rate.

4.3. Variation of the temperature during strain aging

Fig. 11 shows the experimental strain aging results of the ULC bake hardening steel specimens after 5% prestraining for different aging temperatures. The data are plotted as plotted as $\Delta\sigma/\Delta\sigma_{atm}$ vs. aging time, where $\Delta\sigma_{atm}$ is 30 MPa. Again the grain size was about 26 μm for all the specimens. At each aging temperature, the yield stress increment $\Delta\sigma$ reaches a distinct saturation plateau defining the end of the atmosphere formation [3] and then a mild rise in the second stage of bake hardening. This is mainly due to the ultra pure, single-phase matrix of the ULC steel that does not contain any preexisting carbide. This is in agreement with the assumptions of the model to simulate grain boundary segregation during cooling after CA. The same figure shows the degree of dislocation saturation with aging time t predicted by the present model for different aging temperatures. The results show that the model is able to predict complete atmosphere formation. The degree of saturation of the dislocations has an exponential time-dependence and varies almost linearly with the experimental $\Delta\sigma/\Delta\sigma_{atm}$ – aging time relation till the end of the atmosphere formation. At all aging temperatures the predicted behaviour of the dislocation saturation fits excellently well with the experimental aging results of the steel.

4.4. Variation of the prestrain

Fig. 12 shows the evolution of the atmosphere formation with time at 50 °C generated by the present model as a function of varying dislocation density and for solute carbon concentration of 11 ppm (mean carbon concentration in the matrix of the water quenched specimen of grain size 21 μm) respectively. The range of dislocation density used is quite large and includes the amount of the dislocation density normally introduced in specimens during strain aging experiments. It is observed that the degree of atmosphere formation is not influenced by the variation in free dislocation density over this large range. This is valid as long as the solute carbon needed to saturate the mobile dislocations is available in the matrix.

Fig. 13 shows the experimental results of strain aging at 50 °C in specimens prestrained 1–10% with respect to the changes in the increase in yield stress and the yield point elongation (YPE) behaviour. It is seen that the

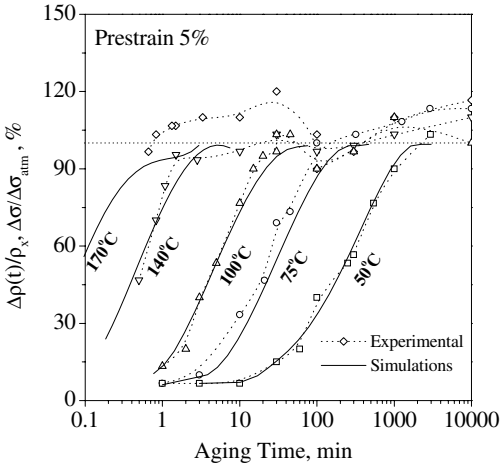

Fig. 11. Measured and calculated normalised yield stress increase as a function of time for different temperatures (Steel B, grain size 26 μm, slow cooling rate, prestrain of 5%).

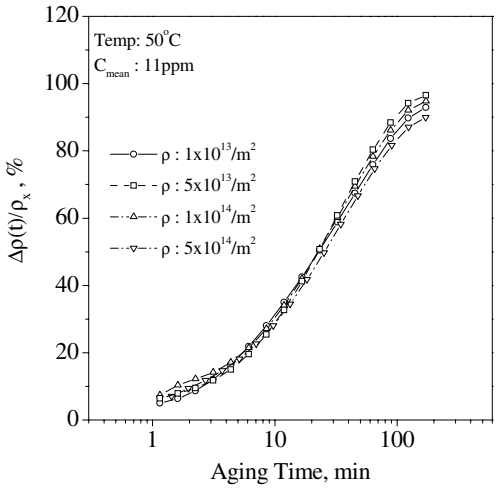

Fig. 12. Calculated dislocation saturation evolutions with aging time (Steel B, grain size 21 μm, water quench, 50 °C) as a function of prestrain.

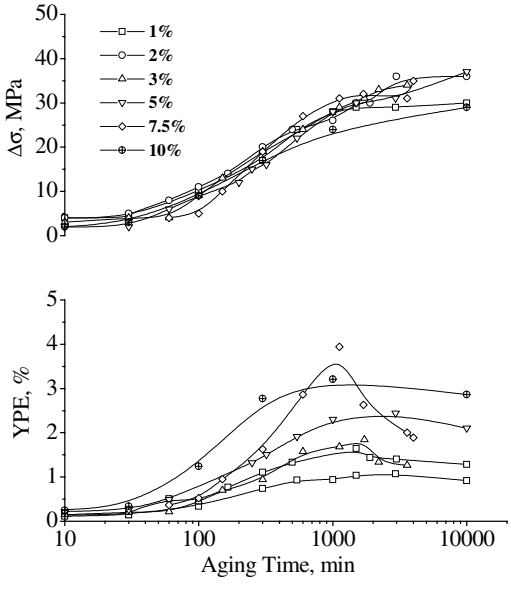

Fig. 13. Increase in the yield stress and yield point elongation (YPE) behaviour with aging time as a function of the amount of prestraining (Steel B, grain size 26 μm, slow cooling cycle, prestrain of 5%).

increase in the yield stress does not distinctly indicate any dependence on the amount of prestraining at any aging time till the completion of the atmosphere formation. The maximum in the yield point elongation is attained almost the same time at all prestrains indicating that the time to complete dislocation locking is not affected by the amount of prestrain. These facts strongly support the numerical simulation results of Fig. 12.

The maximum increase in the yield stress is again ≈30 MPa at all the prestrain levels as indicated by the maximum in the yield point elongation results. However, a mild deviation was observed for the 10% prestrained specimens both in the yield stress increment and the yield point elongation behaviour. This was due to the mutual interference of the dislocations for the available solute contents as the dislocation density increases and also because of low solute contents (6 ppm) in the matrix. It was experimentally observed during amplitude-dependent internal friction measurement and TEM studies that at 10% prestrain, a cellular dislocation structure formed in the present ULC bake hardening steel and it is in agreement with the works of Lan et al. [23].

5. Conclusions

Carbon segregation during CA lowers the solute carbon at the start of strain aging. It is reduced for longer soaking times because the grain size increases, and for higher cooling rates limit the segregation time. Experimental work on an ULC grade with 450 ppm phophorus with internal friction was compared with computer simulations based on finite difference modelling of segregation. For the computer model, a spherical grain approximation was used. Good agreement was obtained when a grain boundary site density of $4/a^2$ to accommodate carbon was used. This value is considerably larger than the values published in literature until now. Carbon segregation to dislocations during strain aging was modelled through the application of diffusion dynamics based on a Monte-Carlo algorithm. The model takes into account the dislocation saturation effects and carbon segregation to the grain boundaries. The degree of atmosphere formation evolved by the model corresponds to the experimental strain aging results of an ultra low carbon bake hardening steel carried out at temperatures 50–170 °C. It was assumed that the increase in the yield stress due to aging varies linearly with the dislocation saturation i.e., the reduction in free dislocation density by carbon atoms. The temperature dependence of the aging process was successfully predicted. It was also clear that variation in the dislocation density over a large range, induced by different prestrains, does not influence the degree of dislocation saturation provided the minimum amount of solute carbon needed to complete atmosphere formation is available in the matrix. Theoretical prediction of dislocation saturation as a function of varying dislocation density was in good agreement to the experimentally observed aging results. These work also revealed that during conventional bake hardening cycles, carbon segregation to grain boundaries is negligible, since the kinetics of this process is much slower than for segregation to dislocations.

References

[1] Cottrell AH, Bilby BA. Proc Phys Soc A 1949;62:49.
[2] Wilson DV, Russell B. Acta Met 1960;8:36.
[3] De AK, Vandeputte S, De Cooman BC. Scripta Mater 1999;41:831.
[4] De AK. Ph.D. Thesis, Ghent University, Belgium; 2001.
[5] Suzuki S, Tanii S, Abiko K, Kimura H. Metall Trans A 1987;18:1109–15.
[6] Cowan JR, Evans HE, Jones RB, Bowen P. Acta Mater 1998;46(18):6565–74.
[7] Suzuki S, Obata M, Abiko K, Kimura H. Trans ISIJ 1985;25:62–8.
[8] McLean S. Grain Boundaries in Metals. Clarendon Press; 1958. Chapter 5.
[9] Grabke H. ISIJ Int 1989;29(7):529.
[10] Grabke H. Steel Res 1986;57(4):178.
[11] Wert C. Phys Rev 1950;79:601.
[12] De AK, Vandeputte S, De Cooman BC. Scripta Mater 2001;44:695.
[13] Kher K, Binder K. Applications of the Monte Carlo method in statistical physics. Berlin: Springer; 1987. p. 181.
[14] Kuhlmann-Wilsdorf D. Metall Trans A 1985;16:2091.
[15] Limoge Y, Bocquet JL. Acta Metall 1988;36:1717.
[16] Zhao L, Najafabadi R, Srolovitz DJ. Acta Metall 1996;44:2737.
[17] Cottrell AH. Report on the strength of solids. Phys Soc 1948:30.
[18] Furusawa K, Tanaka K. J Jpn Inst Met 1969;33(9):985.
[19] Thomas WR, Leak GM. JISI 1955;180:155.
[20] Hartley S. Acta Metall 1966;14:1237.
[21] Ritchie IG, Pan Z. In: 33rd MWSP Conf Proc, vol. 29. Warrendale: ISS; 1992. p. 15.
[22] De AK, Vandeputte S, De Cooman BC. In: 43rd MWSP Conf Proc. Charlotte, NC, October 28–31. ISS; 2001. p. 569–81.
[23] Lan Y, Klaar HJ, Dahl W. Metall Trans A 1992;23:545.
[24] Wert CA, Zener C. Phys Rev 1949;76:1169.
[25] Gladman T. The physical metallurgy of microalloyed steels. The Institute of Materials 1997.
[26] Ray SK. Metall Trans A 1991;22:35–43.
[27] Obara T, Sakata K, Nishida M, Irie T. Kawasaki Steel Techn Rep 1985;12:25–35.